nature neuroscience

A transient network of intrinsically bursting starburst cells underlies the generation of retinal waves

Jijian Zheng[1,2], Seunghoon Lee[1,2] & Z Jimmy Zhou[1]

Pharmacologically isolated starburst amacrine cells (SACs) in perinatal rabbit retinas spontaneously generated semiperiodic calcium spikes and long-lasting after-hyperpolarizations (AHPs), mediated by calcium-activated, cyclic AMP–sensitive potassium currents. These AHPs, rather than a depletion of neurotransmitters (as was previously believed), produced the refractory period of spontaneous retinal waves and set the upper limit of the wave frequency. Each SAC received inputs from roughly 10–30 neighboring SACs during a wave. These inputs synchronized and reshaped the intrinsic bursts to produce network oscillations at a rhythm different from that of individual SACs. With maturation, the semiperiodic bursts in SACs disappeared, owing to reduced intrinsic excitability and increased network inhibition. Thus, retinal waves are generated by a transient and specific network of cell-autonomous oscillators synchronized by reciprocally excitatory connections.

Retinal waves are semiperiodic bursts of excitation occurring spontaneously in the developing retina of all vertebrate species that have been examined thus far[1,2]. Although the exact functions of retinal waves are yet to be elucidated, increasing evidence from recent studies suggests that the waves have a critical role in the establishment of precise retinofugal pathways and that certain spatiotemporal properties of the waves may encode specific developmental cues[3–8]. However, despite more than a decade of intense investigation, the mechanism responsible for retinal wave generation remains largely a hypothesis. According to the prevailing theory[9] adapted from other developing nervous systems (for example, the spinal cord[10]), retinal waves are initiated by random local perturbations in an early recurrent network without a well-defined pacemaker circuit, and the spatiotemporal pattern of the waves is shaped by a refractory process governed by network depression, such as synaptic depression caused by the depletion of the readily releasable pool of neurotransmitters. This theory (referred to as 'recurrent network theory' henceforth) for early network oscillations in the developing retina is different from the classic pacemaker model[11–13] for most neuronal oscillations in the mature nervous system in that it emphasizes the network origin of wave initiation and network homeostasis for rhythmogenesis.

The recurrent network theory for retinal waves is based mainly on three lines of observation. First, rhythmic activity has never been found in the developing retina in the presence of pharmacological agents that abolish retinal waves[1], arguing against the presence of cell-autonomous pacemakers. Second, the rhythm of retinal waves ($\sim 10^{-2}$ Hz; refs. 1,9) is much slower than the oscillation frequencies in most mature nervous systems[12,13]. This argues against a refractory mechanism based on conventional AHP or ion channel activation or inactivation; instead, it favors network homeostatic processes, such as the depletion of releasable neurotransmitters[10]. Third, the recurrent network theory provides an attractive explanation for the eventual disappearance of retinal waves based on the developmental transitions in network excitability (see below; ref. 14), whereas it is not known why low frequency pacemakers, if they existed during development, are not seen in the mature retina. However, all of the above observations have been made only in general terms and have never been rigorously tested. Consequently, the recurrent network theory has remained mysteriously vague, with no specific mechanisms to account for such important concepts as local perturbation and network homeostasis.

Retinal waves in mammals develop through three stages[15,16]. Stage II waves are so far the best characterized and appear in rabbits between embryonic day 24 (E24) and postnatal day 3–4 (P3–4; ref. 15). Because these waves are driven by nicotinic neurotransmission[16–19], it is believed that cholinergic (starburst) amacrine cells[20] have a critical role in stage II wave formation[21]. In a previous study, we established that SACs make reciprocal nicotinic and GABAergic synapses onto each other and that mutual nicotinic excitation within the SAC network drives SACs to burst during retinal waves[14]. As retinal waves progress from stage II to stage III, the nicotinic synapses between SACs are sharply reduced and the GABAergic synapses switch from excitatory to inhibitory[14]. These results demonstrate that in agreement with the recurrent network theory, there is indeed a transient recurrent network formed by SACs, such that once the activity is set in motion, the network is able to mediate retinal waves. However, a fundamental question regarding the origin of retinal waves remains unanswered: how does this network generate retinal waves and produce the wave rhythm?

Here we report that stage II retinal waves in rabbits originated from cell-autonomous bursts of SACs and that the refractory process was

[1]Department of Physiology and Biophysics and Department of Ophthalmology, University of Arkansas for Medical Sciences, Little Rock, Arkansas 72205, USA.
[2]These authors contributed equally to this work. Correspondence should be addressed to Z.J.Z. (zhoujimmy@uams.edu).

Received 1 December 2005; accepted 18 January 2006; published online 5 February 2006; doi:10.1038/nn1644

dictated by a slow AHP, which together with network interactions generated the wave rhythm.

RESULTS

The cell-autonomous activity in developing SACs

When recorded under whole-cell current clamp in the whole-mount perinatal rabbit retina, displaced SACs underwent semiperiodic bursts of spikes and prolonged AHPs (**Fig. 1a**,**b**). These bursts were of two related types. The first type, defined as a compound burst, consisted of spikes riding atop an excitatory postsynaptic potential (EPSP, **Fig. 1a**, left inset), which had a waveform similar to that of the rhythmic synaptic currents in SACs recorded under voltage clamp (**Fig. 1c**, inset). This indicated that this type of burst coincided with the synaptic excitation during a spontaneous retinal wave. Dual patch-clamp recording from neighboring SACs and ganglion cells (**Fig. 1d**) also confirmed that the compound bursts in SACs were closely correlated with the rhythmic bursts in ganglion cells. The second type of burst, defined as a simple or intrinsic burst, was similar to the first type, except that it did not contain the EPSP component (**Fig. 1a**, right inset). Compared to compound bursts, simple bursts were usually followed by a shorter AHP and, on rare occasions, contained only a few brief spikes without a prominent AHP (**Fig. 1d**, asterisks). Simple bursts typically appeared long after (>20 s) a compound burst and were not synchronized with the spikes in neighboring cells (**Fig. 1d**), suggesting that they were not associated with retinal waves. Dual patch-clamp recording from SAC and ganglion cell pairs found prolonged AHPs in SACs but not in the ganglion cells tested (**Fig. 1d**, inset).

To distinguish whether the rhythmic bursts in SACs originate from cell-autonomous activities or from network interactions, we isolated SACs pharmacologically by adding, to the physiological solution (Ames

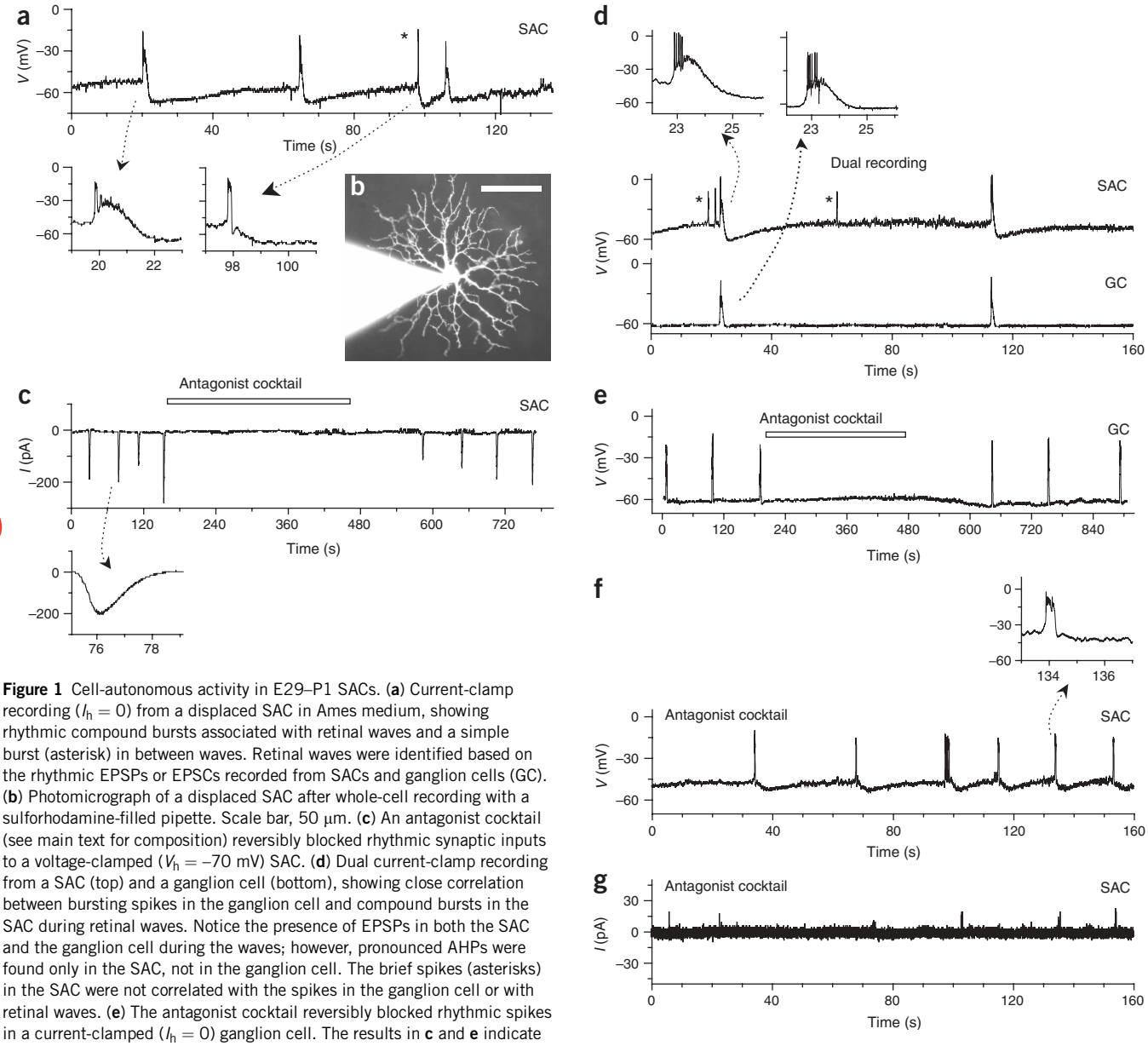

Figure 1 Cell-autonomous activity in E29–P1 SACs. (**a**) Current-clamp recording ($I_h = 0$) from a displaced SAC in Ames medium, showing rhythmic compound bursts associated with retinal waves and a simple burst (asterisk) in between waves. Retinal waves were identified based on the rhythmic EPSPs or EPSCs recorded from SACs and ganglion cells (GC). (**b**) Photomicrograph of a displaced SAC after whole-cell recording with a sulforhodamine-filled pipette. Scale bar, 50 μm. (**c**) An antagonist cocktail (see main text for composition) reversibly blocked rhythmic synaptic inputs to a voltage-clamped ($V_h = -70$ mV) SAC. (**d**) Dual current-clamp recording from a SAC (top) and a ganglion cell (bottom), showing close correlation between bursting spikes in the ganglion cell and compound bursts in the SAC during retinal waves. Notice the presence of EPSPs in both the SAC and the ganglion cell during the waves; however, pronounced AHPs were found only in the SAC, not in the ganglion cell. The brief spikes (asterisks) in the SAC were not correlated with the spikes in the ganglion cell or with retinal waves. (**e**) The antagonist cocktail reversibly blocked rhythmic spikes in a current-clamped ($I_h = 0$) ganglion cell. The results in **c** and **e** indicate the blockade of spontaneous retinal waves and the wave-associated synaptic inputs to the SAC. (**f**,**g**) Cell-autonomous rhythmic bursts persisted in the presence of the antagonist cocktail in (**f**) a whole-cell current-clamped ($I_h = 0$) SAC and (**g**) an on-cell, loose patch-clamped SAC ($V_h = 0$ mV).

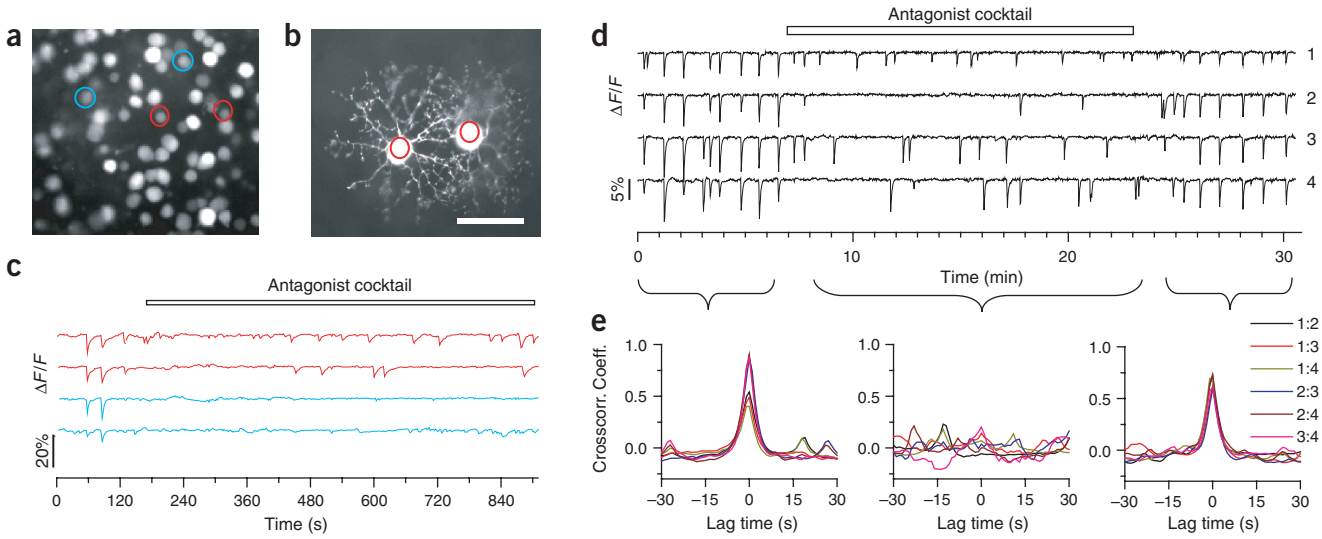

Figure 2 Cell-autonomous activities of SACs under Ca^{2+} imaging. (**a**) Ca^{2+} imaging from ganglion cells and displaced amacrine cells loaded with Fura2-AM in a P0 retina. Cells with larger somas (for example, circled in blue) were presumably ganglion cells. (**b**) Two smaller cells (circled in red in **a**) were identified as SACs by Lucifer yellow injection after Ca^{2+} imaging. (**c**) An antagonist cocktail blocked spontaneous waves (synchronous downward deflections) and all activities in the ganglion cells (blue traces, measured from the blue circles in **a**) but spared the intrinsic activity in the SACs (red traces, measured from the red circles in **a**). (**d**) Ca^{2+} imaging from four neighboring SACs (marked 1–4) in a P1 retina under the control, antagonists (100 μM hexamethonium and 100 μM picrotoxin) and wash-out conditions. (**e**) Overlay of cross-correlograms for the six possible pairwise comparisons of the four traces in **d**, showing a high level of correlation near a lag time of 0 s, which was reversibly abolished by the antagonists. Because asynchronous, independent oscillators of similar intrinsic frequencies may still exhibit a certain degree of correlation, small 'bumps' in the cross-correlation coefficient (<0.25) were still visible at random lag times for some pairs of SACs in the presence of the antagonists. Scale bar, 50 μm.

medium; ref. 22), an antagonist cocktail consisting of 75 μM 18β-glycyrrhetinic acid, 100 μM hexamethonium, 40 μM 6-cyano-7-nitroquinoxaline-2,3-dione (CNQX), 200 μM AP7 (D(-)-amino-7-phosphonoheptanoic acid), 100 μM picrotoxin, 2 μM strychnine and 1 μM atropine. This cocktail blocks common electric and chemical synapses in the retina, including those that are essential for stage I (gap junction), stage II (nicotinic receptors) and stage III (glutamate and muscarinic receptors) retinal waves in rabbits[18]. Notably, although this cocktail completely abolished both the rhythmic spikes in current-clamped ganglion cells (**Fig. 1e**, $n = 6$) and the rhythmic synaptic current in voltage-clamped SACs (**Fig. 1c**, $n = 25$), it did not block the rhythmic bursts or the characteristic AHPs in SACs under current clamp (**Fig. 1f**, $n = 8$). This indicated that these bursts and AHPs were cell-autonomous activities independent of network interactions. We also observed similar intrinsic bursts in the presence of the nicotinic blocker hexamethonium alone (which is sufficient to block stage II waves and the associated rhythmic synaptic inputs to SACs (refs. 15,18, $n = 12$) and hexamethonium together with picrotoxin ($n = 10$), suggesting that these bursts were not induced artificially by the combination of the antagonists. To rule out the possibility that whole-cell current-clamp recording might have inadvertently induced bursts by altering the excitability of the cell, we also recorded from SACs using on-cell, loose patch clamp and observed similar bursts of spikes in the presence of the antagonist cocktail (**Fig. 1g**, $n = 5$). Finally, calcium imaging from the ganglion cell layer of retinas loaded with Fura-2AM ($n = 9$ retinas, **Fig. 2a**,**b**) showed that the antagonist cocktail blocked correlated spontaneous waves but spared the cell-autonomous activities in SACs (**Fig. 2c**,**d**). Under the control condition, the cross-correlograms between neighboring SACs showed a sharp peak around a lag time of 0 s, indicating a high level of synchrony (**Fig. 2e**, left). However, this synchrony was reversibly abolished by the hexamethonium together with picrotoxin (**Fig. 2e**, center and right). Similar results were obtained from four other retinas (**Supplementary Fig. 1** online).

In the presence of the antagonist cocktail, all bursts in SACs became simple bursts (**Fig. 1f**, $n = 18$), as expected because retinal waves and the rhythmic synaptic inputs (EPSPs) associated with the waves were blocked under this condition. Under whole-cell patch clamp, the distribution of interburst interval (**Fig. 3a**) in the cocktail had an interval of 15 ± 7s (mean ± s.d.; $n = 68$). These bursts were semiperiodic, and the interval between two successive bursts varied in a wide range, from <10 s to 40 s (median: 13 s). A similar interburst interval distribution (mean ± s.d.: 19 ± 16 s; median: 14 s, $n = 26$) was obtained by on-cell, loose patch recording, but the variability in interburst interval was larger, ranging from <10 s to 80 s (**Fig. 3b**). The median interburst interval measured by either whole-cell or on-cell recording in the cocktail was substantially shorter than the median interwave interval measured in Ames medium (**Fig. 3c**). Under our recording condition, semirhythmic bursts were detected in about 60% (90 of ~150) of the SACs tested under whole-cell clamp, although it is likely that this percentage is an underestimate of the actual SACs having intrinsic bursts (Discussion).

Mechanisms underlying the intrinsic activity in SACs

The bursting spikes in SACs were generated mainly by voltage-gated calcium (Ca^{2+}) currents, because 0.3 mM cadmium (Cd^{2+}) blocked both the spontaneous rhythmic activity ($n = 8$, data not shown) and the repetitive spikes evoked by depolarizing current steps (**Fig. 4a**, $n = 6$). To simulate the spikes during a spontaneous wave, we first recorded synaptic currents from a voltage-clamped SAC during a spontaneous wave (similar to that in **Fig. 1c** inset) and then injected these currents (referred to as 'wave currents' henceforth) back into the SACs under current clamp (**Fig. 4b–e**, top). This resulted in a voltage response that closely resembled the compound burst found during a spontaneous

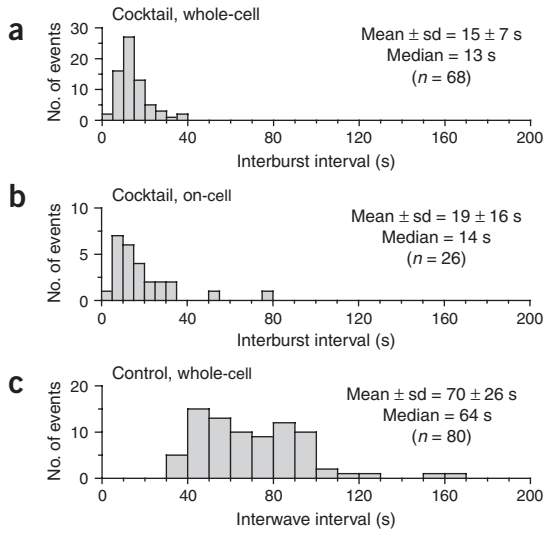

Figure 3 Temporal properties of the bursts in SACs. (**a**,**b**) Distributions of interburst interval in the presence of the antagonist cocktail recorded from SACs under (**a**) whole-cell patch clamp ($I_h = 0$) and (**b**) on-cell loose clamp. (**c**) Interwave interval distribution for spontaneous waves measured from SACs under whole-cell patch clamp in Ames medium. The waves were identified on the basis of the presence of the characteristic EPSCs or EPSPs under whole-cell patch clamp.

wave, with repetitive spikes riding atop a slow depolarization potential, followed by a prominent AHP (**Fig. 4b–e**, bottom). Tetradotoxin (TTX; 1 μM) did not block the repetitive spikes evoked by wave currents or the characteristic AHP (**Fig. 4b**), although the kinetics, amplitude and threshold of the spikes were slightly altered (**Fig. 4c**). Cd^{2+} (0.3 mM, **Fig. 4d**, $n = 6$) blocked these spikes and AHPs whereas cesium (Cs^+; 5 mM, **Fig. 4e**, $n = 4$) did not, revealing the involvement of Ca^{2+} and Ca^{2+}-activated currents but not the conventional Cs^+-sensitive pacemaker current (I_H; ref. 11) (which was hardly detectable under voltage clamp; **Fig. 4f**) in the generation of the bursts and AHPs.

The AHP following a burst of spikes in the SACs varied in amplitude with the membrane holding potential and reversed its polarity (that is, became depolarizing) when the cells were held below the potassium (K^+) equilibrium potential E_K (–92 mV; **Fig. 4g**). This suggested that the AHP was mediated mainly by a K^+ conductance, most probably a slowly inactivating, Ca^{2+}-activated K^+ conductance. Indeed, flash photolysis of caged Ca^{2+} (DM-nitrophen, dialyzed into SACs from patch pipettes) evoked a slowly decaying outward current under voltage clamp at –60 mV (**Fig. 4h**, $n = 10$). This current reversed at E_K (–92 mV, **Fig. 4i**, $n = 4$), consistent with a Ca^{2+}-activated, voltage-independent K^+ current. A similar current was also evoked by depolarizing pulses (**Fig. 4h**, $n = 15$) and were blocked by Cd^{2+} (data not shown). Notably, the Ca^{2+}-activated K^+ current in SACs was sensitive to intracellular cyclic AMP (cAMP). Flash photolysis of caged cAMP (dialyzed into SACs via patch pipettes) caused a marked reduction of this current under voltage clamp (data not shown) and a rapid truncation of the AHP under current clamp (**Fig. 4j**, $n = 4$). Similarly, the application of the adenylate cyclase activator forskolin (1 μM) reduced the amplitude and decay time of the AHP and increased the frequency of spontaneous waves (**Fig. 4k**, $n = 4$). Forskolin increases retinal wave frequency[23] and, when injected monocularly, alters eye-specific segregation in retinogenicular projections[3]. Thus, our results (**Fig. 4**) provide the first cellular mechanism for this important effect of forskolin on spontaneous retinal waves, although forskolin may also influence the dynamics of retinal waves by affecting other cell types that participate in the waves.

In contrast, both the Ca^{2+}-activated K^+ conductance (activated by voltage pulses) and the slow AHP (evoked either during a wave or by wave currents) in SACs were insensitive to charybdotoxin and apamin (50 nM and 300 nM, respectively; both $n = 8$; data not shown). This ruled out the involvement of the large conductance (BK) and apamin-sensitive small-conductance (SK) Ca^{2+}-activated K^+ channels[24]. Based on its pharmacology, slow kinetics and sensitivity to cAMP, the Ca^{2+}-activated K^+ current in SACs seemed similar to the slow AHP currents (I_{sAHP}) reported in hippocampal pyramidal neurons[25–30] although clotrimazole (20 μM), which blocks I_{sAHP} in cultured hippocampal pyramidal cells[31], did not block this current in SACs ($n = 6$, data not shown). Taken together, our results suggested that the rhythmic activity in pharmacologically isolated SACs was mediated predominantly by voltage-gated Ca^{2+} currents and a slow Ca^{2+}-dependent, cAMP-sensitive K^+ current resembling I_{sAHP}. The decay of this Ca^{2+}-activated K^+ current had a major role in the recovery phase of the AHP, although it is possible that other currents might have contributed to the spikes and AHP to a lesser degree (see Discussion).

ACh was not depleted during the refractory period

To further understand the mechanism of rhythmogenesis for retinal waves, we tested a widely held theory that the refractory process following a wave is caused by the depletion of readily releasable neurotransmitters. Because stage II retinal waves in the rabbit rely critically on the release of acetylcholine (ACh) from SACs (ref. 14) and are not affected by GABA receptor blockers[15], we directly compared the efficacy of cholinergic synaptic transmission between SACs shortly before and immediately after a spontaneous retinal wave under dual patch clamp. The SAC being tested for ACh release (referred to as the presynaptic cell) was held under current clamp (holding cation current $I_h = 0$), except during brief moments when a voltage pulse (–70 mV to 15 mV) was given under voltage clamp to evoke transmitter release. The neighboring SAC used to detect ACh release (referred to as the postsynaptic cell) was held constantly at –70 mV (E_{Cl}) to isolate the nicotinic current input. We found that presynaptic voltage steps given shortly before and immediately after a spontaneous wave evoked similar postsynaptic responses (**Fig. 5a**, $n = 6$), arguing against the transmitter depletion theory.

To confirm the above finding, we used a paired-pulse protocol to simulate two successive waves in the presynaptic cell with two injections of wave currents under current clamp, while comparing the responses of the postsynaptic cell under voltage clamp at –70 mV (**Fig. 5b**). Under this condition, we did find paired-pulse depression (that is, reduced neurotransmission during the second stimulation as measured by the integral of inward postsynaptic nicotinic currents; **Fig. 5b**). However, this paired-pulse depression was due, mainly, to the I_{sAHP} activated by the first stimulation, which prevented the second stimulation from evoking suprathreshold Ca^{2+} spikes (**Fig. 5b**). It was not due to a depletion of releasable transmitter, because the depression could be eliminated when the amplitude of the two pulses was made large enough to evoke a suprathreshold burst during both the first and the second pulse (**Fig. 5c**). The I_{sAHP} produced the AHP, thereby keeping the cell farther away from the spike threshold; it also reduced the membrane input resistance (and hence the amplitude of depolarization by the subsequent current input), making it more difficult for the cell to generate spikes (**Supplementary Fig. 2** online). In addition to I_{sAHP} activation, other factors, such as the inactivation of presynaptic Ca^{2+} channels and the desensitization of postsynaptic nicotinic receptors during the burst, might also

contribute to the initial phase of the refractory process but such factors do not seem responsible for the prolonged refractory period. Together, these results demonstrated that the refractory period of retinal waves was determined mainly by the time course of the AHP, not by a depletion of releasable ACh.

The interplay between intrinsic and network activities

To determine whether synaptic interactions in the SAC network have a role in rhythmogenesis of retinal waves, we compared the rhythmic bursts of SACs recorded in Ames medium with those recorded in the presence of the antagonist cocktail. Without network interaction (in the cocktail), the AHP following an intrinsic burst (**Fig. 1f**) had a mean duration of 14 ± 7 s (n = 68), which closely matched the average interburst interval (15 ± 7 s, n = 68, **Fig. 3a**), suggesting that the intrinsic AHP dictated the interburst interval under this condition. However, with network interactions intact (in Ames medium), SACs received a barrage of synaptic inputs during each wave (**Fig. 1c**). Bursts occurring during the waves were reshaped by network interactions, which added an EPSP component to the bursts (**Fig. 6a**) and prolonged the mean AHP duration to 28 ± 6 s (n = 36). To determine whether this EPSP prolonged the AHP by increasing the intracellular Ca^{2+}, we compared the Ca^{2+} influx during an intrinsic burst (**Fig. 6a**, left) with that during a compound burst (**Fig. 6a**, right). We used prerecorded waveforms of intrinsic and compound bursts (**Fig. 6b**, top) as voltage commands to activate Ca^{2+} currents in SACs under voltage clamp (**Fig. 6b**, middle). We found that the presence of an EPSP nearly doubled the Ca^{2+} influx during a burst (**Fig. 6b**, bottom), a result that was supported by Ca^{2+} imaging from SACs loaded with Fura-2AM (**Fig. 6c**). Thus, network interactions enhanced the Ca^{2+} entry and prolonged the AHP. It is possible that the regulation of AHP by the network may involve additional second messengers (for example, cAMP) and ion channels.

The average AHP duration (28 s ± 6 s, n = 36) following a compound burst closely matched the minimum interval between

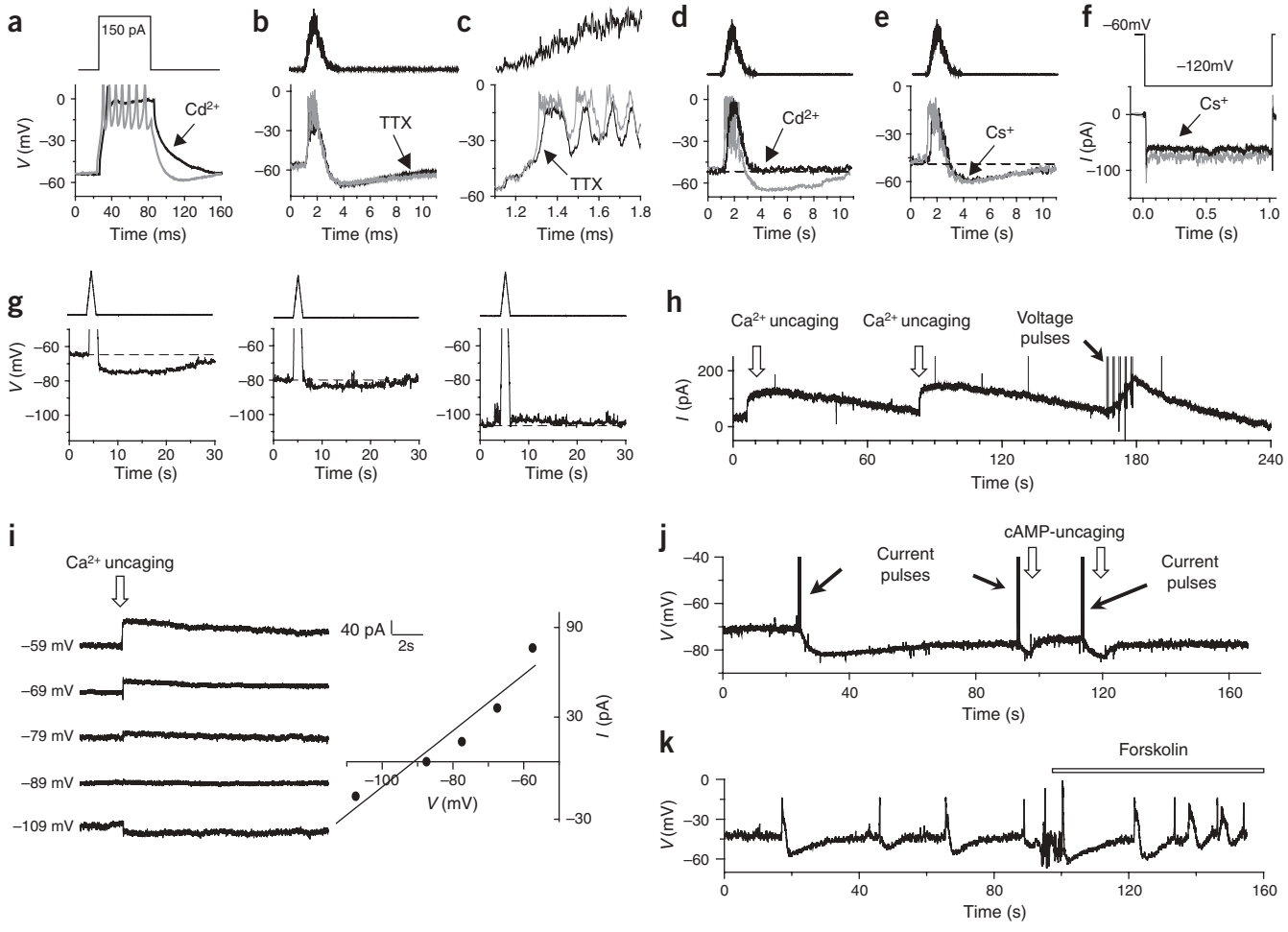

Figure 4 The ionic mechanism of intrinsic bursts in SACs. (**a**) Repetitive Ca^{2+} spikes and the subsequent AHP evoked under current clamp (I_h = 0; gray). $CdCl_2$ (0.3 mM) blocked the repetitive spikes and AHP, sparing an initial Na^+ spike (black). (**b**) Injection of wave currents (top, prerecorded at –70 mV during a spontaneous wave) under current clamp (I_h = 0) evoked spikes and an AHP that resembled those during a compound burst (gray). TTX did not block the spikes or the AHP (black). (**c**) Blown-up view of the spikes in **b**, showing some reduction, by TTX, of the depolarization rate and amplitude of the spikes. (**d**,**e**) Application of Cd^{2+} (0.3 mM, **d**), but not Cs^+ (5 mM, **e**), completely blocked the repetitive Ca^{2+} spikes and the characteristic AHP evoked by the wave currents. (**f**) Hyperpolarization under voltage clamp did not detect any Cs^+-sensitive I_H current. (**g**) The amplitude of AHP (evoked by current ramps shown on the top) varied with the holding potential and reversed in polarity near –92 mV (E_K). (**h**) Flash photolysis (1 ms duration) of DM-nitrophen evoked a Ca^{2+}-activated outward current under voltage clamp at –60 mV, resembling the current evoked by voltage pulses (–60 mV to +5 mV). (**i**) I-V relation of the currents evoked by Ca^{2+} uncaging, showing a reversal potential at –92 mV (E_K). (**j**) Flash photolysis of caged cAMP rapidly truncated the AHPs evoked by depolarizing current pulses. (**k**) Forskolin (1 μM) reduced the amplitude and decay rate of the AHPs that followed both the compound and simple bursts under current-clamp (I_h = 0).

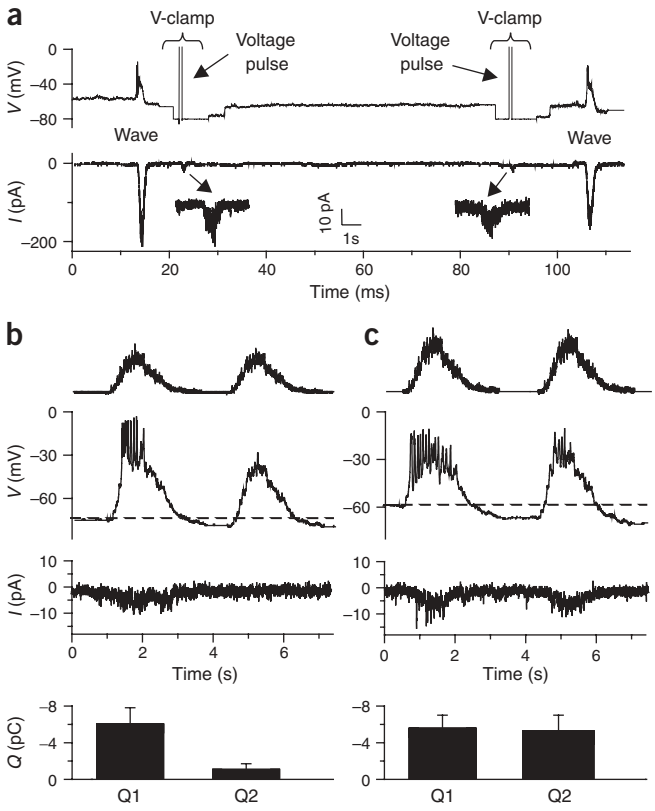

Figure 5 Mechanism of the postwave refractory process. (**a**) Dual patch clamp from a pair of SACs, showing similar synaptic transmission evoked immediately after and shortly before a spontaneous wave. The presynaptic cell was current clamped ($I_h = 0$), except for brief moments during which a voltage pulse (–70 mV to +15 mV) was applied under voltage clamp to evoke synaptic release. The current-clamp condition allowed the presynaptic cell to participate in the normal process of rhythmic excitation, including the compound burst of spikes and the subsequent refractory process, whereas the brief voltage pulses under voltage clamp enabled the cell to be depolarized to the same level for consistent comparison of transmitter release. The postsynaptic cell was voltage clamped at –70 mV. (**b**) Two-pulse wave current stimulation during dual patch clamp from SACs. The first pulse (top left) evoked suprathreshold spikes in the presynaptic cell (current-clamped with $I_h = 0$, middle left) and nicotinic[14] currents in the postsynaptic cell (voltage-clamped at –70 mV, bottom left). The second pulse (top right) did not evoke suprathreshold, presynaptic spikes (middle right) or postsynaptic currents (bottom right). The histograms denote integrals of postsynaptic currents (averaged from five starburst pairs), showing reduced synaptic transmission during the second pulse. Q1and Q2 represent average charge transfer associated with the postsynaptic current during the first and second stimulation, respectively. (**c**) With increased amplitude of the two pulses, suprathreshold spikes and postsynaptic responses could be evoked by both pulses, eliminating the paired-pulse depression (see histogram, $n = 5$). Error bars represent s.d.

spontaneous waves (~30 s, **Fig. 3c**), suggesting that the AHP largely dictated the postwave refractory period and the upper limit of the wave frequency. However, this mean AHP duration was shorter than the mean interwave interval (70 ± 26, $n = 80$, **Fig. 3c**), indicating that cell-autonomous bursts in SACs alone cannot account for the entire mechanism of rhythmogenesis for retinal waves. This is consistent with our observation that in addition to compound bursts that were synchronized with the waves, there were asynchronous intrinsic bursts between waves (**Fig. 1a** and **Fig. 6e**). Dual on-cell and whole-cell patch clamp from SAC-SAC and SAC–ganglion cell pairs also confirmed the presence of asynchronous intrinsic bursts (**Fig. 6d**). This suggested that these asynchronous bursts were not an artifact caused by the whole-cell recording condition (although we cannot rule out the possibility that whole-cell recording might have influenced the membrane potential and the AHP duration to some extent, thereby altering the frequency of asynchronous bursts; see Discussion). These results suggested that not every burst in a SAC was associated with the initiation of a retinal wave and that the generation of a wave requires a certain level of synchrony among intrinsically bursting SACs.

We next examined whether network interactions influenced the synchrony among bursting SACs. The number of intrinsic bursts between two successive waves varied from wave to wave and from retina to retina (**Fig. 6e**,**f**). Reducing the recurrent interaction among SACs with a low concentration of hexamethonium (10 μM) markedly decreased the wave frequency and increased the number of asynchronous intrinsic bursts between waves (**Fig. 6g**), suggesting that network interactions increased the synchrony among SACs, perhaps by bringing more cells simultaneously to the spike threshold by means of the EPSP. When the level of synchrony was high, most bursts were associated with the waves (compound bursts) and the interwave interval approached the AHP duration that followed a compound burst (**Fig. 6f**). In contrast, when the network interaction was completely blocked by the cocktail, SACs became independent of each other and we no longer saw waves (**Fig. 1f**).

To gain a clue to the degree of synchrony among SACs during a retinal wave, we used dual patch clamp to compare the total nicotinic input[14] (150–300 pA in peak amplitude, **Fig. 6h**, bottom left) received by a SAC during a spontaneous wave with the nicotinic synaptic current (10–15 pA in peak amplitude, **Fig. 6h**, bottom right) received from a single neighboring SAC, which experienced a 'simulated wave' evoked by an injection of wave currents (**Fig. 6h**, top right). Based on the simplest assumption of linear summation, we estimate that a SAC received synaptic inputs from approximately 10–30 neighboring SACs during a spontaneous wave (see Discussion). Indeed, a summation of 20 such inputs from a single neighboring SAC (pooled from 10 paired recordings) resulted in a postsynaptic current (**Fig. 6h**, inset) that closely resembled the total synaptic input received by a SAC during a spontaneous wave.

The transient appearance of the intrinsic activity in SACs

To determine how the intrinsic activity in SACs evolves during retinal development, we recorded from SACs at various ages from E29 (2 d before birth) to P29. The intrinsic bursts in SACs remained until P4 (**Fig. 7a**) but became undetectable after P6 (**Fig. 7b**, top). At P4, five out of six SACs tested showed the characteristic intrinsic bursts. However, none of the P6 ($n = 6$) and older ($n = 25$) SACs that we recorded from showed such activity.

We found that in the presence of the antagonist cocktail, tetraethylammonium (TEA; 1mM) effectively induced rhythmic activities in older (>P7) SACs (**Fig. 7b**, bottom). Because TEA presumably increased the excitability of older SACs by blocking K^+ channels, particularly the K_{V3} types which are expressed in the proximal region of mature SACs and are sensitive to low concentrations of TEA (ref. 32), the loss of the rhythmic bursting activity seemed to have been caused by a developmental reduction in the intrinsic excitability of SACs. Notably, however, TEA (1 mM) alone without the antagonist cocktail could not induce the rhythmic activity (**Fig. 7c**, top); neither could the cocktail alone without TEA (**Fig. 7b**, top). This suggested that network interactions in the older retina (particularly the GABAergic inhibition

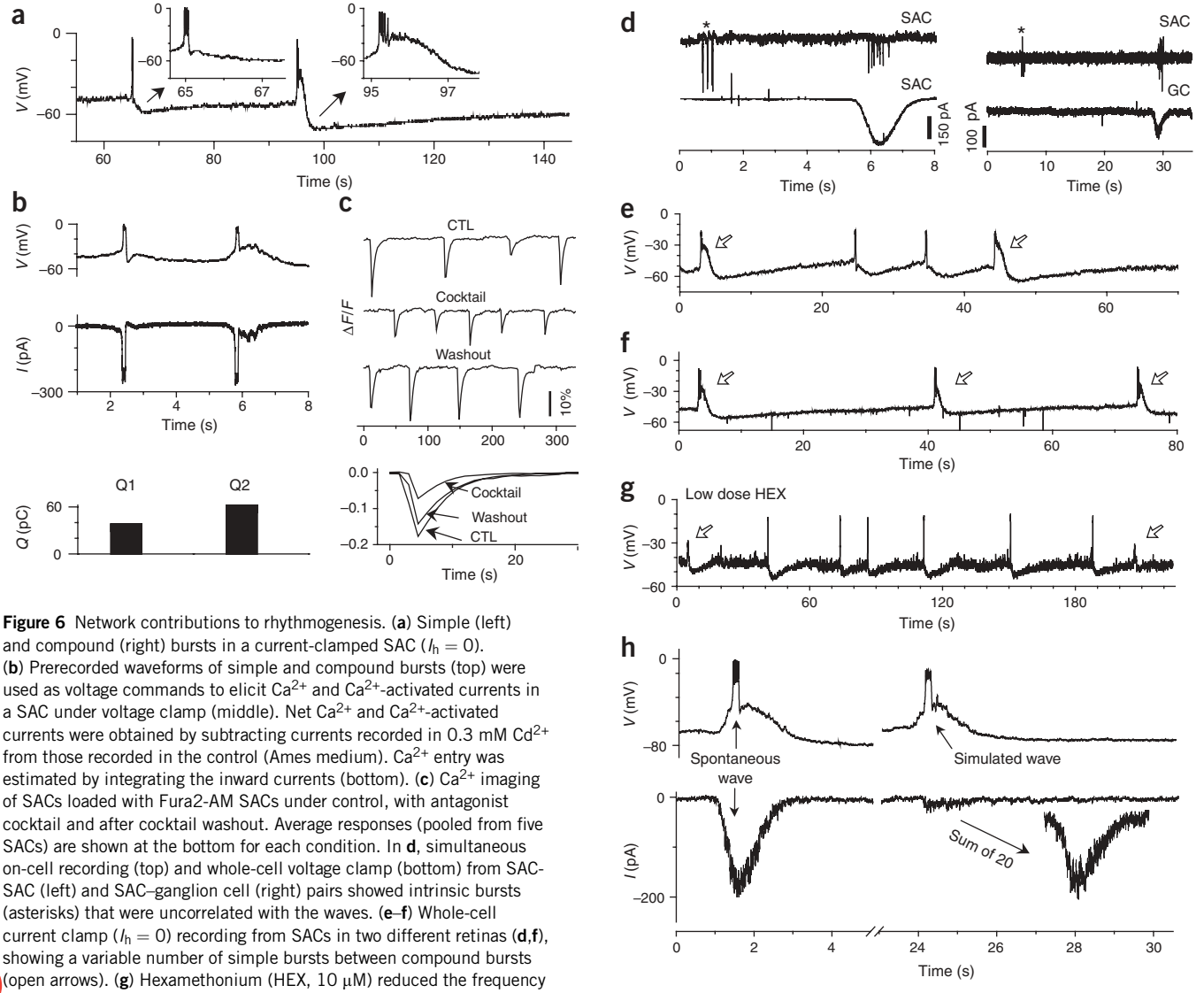

Figure 6 Network contributions to rhythmogenesis. (**a**) Simple (left) and compound (right) bursts in a current-clamped SAC ($I_h = 0$). (**b**) Prerecorded waveforms of simple and compound bursts (top) were used as voltage commands to elicit Ca^{2+} and Ca^{2+}-activated currents in a SAC under voltage clamp (middle). Net Ca^{2+} and Ca^{2+}-activated currents were obtained by subtracting currents recorded in 0.3 mM Cd^{2+} from those recorded in the control (Ames medium). Ca^{2+} entry was estimated by integrating the inward currents (bottom). (**c**) Ca^{2+} imaging of SACs loaded with Fura2-AM SACs under control, with antagonist cocktail and after cocktail washout. Average responses (pooled from five SACs) are shown at the bottom for each condition. In **d**, simultaneous on-cell recording (top) and whole-cell voltage clamp (bottom) from SAC-SAC (left) and SAC–ganglion cell (right) pairs showed intrinsic bursts (asterisks) that were uncorrelated with the waves. (**e**–**f**) Whole-cell current clamp ($I_h = 0$) recording from SACs in two different retinas (**d**,**f**), showing a variable number of simple bursts between compound bursts (open arrows). (**g**) Hexamethonium (HEX, 10 μM) reduced the frequency of compound bursts and increased the number of simple bursts between two successive waves (open arrow). (**h**) Simultaneous recording from two neighboring SACs under current clamp (top, $I_h = 0$) and voltage clamp (bottom, $V_m = -70$ mV), respectively. Bottom left, synaptic inputs received by the voltage-clamped SAC during a spontaneous wave. Bottom right, synaptic input received when the neighboring SAC (top) was stimulated by wave currents. Inset, summation of 20 postsynaptic responses (from 10 paired recordings) during 'simulated waves'.

between >P6 SACs; ref. 14) also had a role in preventing the bursts from occurring.

DISCUSSION

Mechanisms underlying retinal waves

This study resulted in five main findings: (i) SACs generated semiperiodic, intrinsic bursts; (ii) a slow AHP in SACs produced the postwave refractory period; (iii) the releasable pool of ACh was not depleted during the refractory period; (iv) the interplay between intrinsic SAC oscillations and network interactions underlay the initiation and rhythmogenesis of retinal waves; and (v) the intrinsic spikes in SACs existed during a transient developmental period. These results identified the cell-autonomous activity in SACs as the main source of the excitation during retinal waves and the AHP in SACs as the main cause of the refractory period. Together, the above findings revealed a mechanism whereby cell-autonomous oscillators, synchronized by a recurrently excitatory network, underlie the generation of spontaneous retinal waves. This new mechanism may also shed light on the genesis of early network oscillations in other developing nervous systems, such as the hippocampus[33].

Our recordings so far have not provided convincing evidence that stimulating a single SAC under patch clamp can generate a wave. It seems that the initiation of a wave may depend on the probability that a certain number of neighboring SACs spike nearly synchronously and that many other neighboring SACs are ready to be recruited into a wave. The degree of synchrony seems to depend on network interactions, particularly the reciprocal excitatory synaptic interactions among SACs (ref. 14). We found that network interactions contributed to rhythmogenesis in at least two important ways. First, they amplified the intrinsic burst and prolonged the AHP in individual SACs. Second, they controlled the synchrony among SACs and influenced the probability of wave initiation. We estimated, based on the simplest

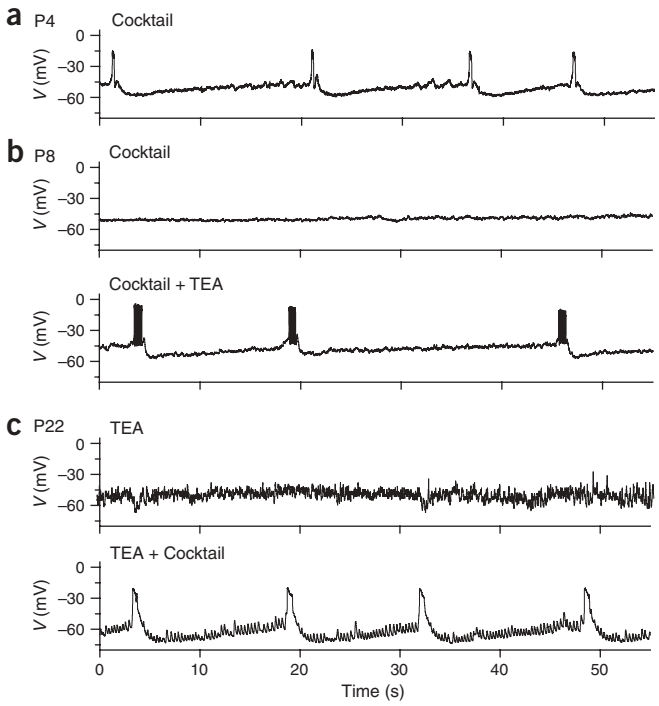

Figure 7 Developmental loss of intrinsic bursts in SACs. (**a**) Rhythmic activity detected from a P4 SAC in the presence of the antagonist cocktail. (**b**) No intrinsic rhythmic activity was found in a P8 SAC in the cocktail. Addition of 1 mM TEA induced robust rhythmic activity in the same cell. (**c**) TEA (1 mM) alone was ineffective in inducing pacemaker activity in a P22 starburst cell, but additional synaptic blockade by the cocktail induced rhythmic activities in the same cell.

assumption of linear summation, that each SAC received synaptic inputs from roughly 10–30 overlapping SACs during a spontaneous wave. However, if reciprocal excitation among SACs is taken into consideration, the actual number of contributing SACs is expected to be smaller. Because SACs are known to have a very high overlapping factor[34–36], our results suggest that a variable fraction of the total number of overlapping SACs may be synchronized during a wave. Thus, by modulating the strength of the interaction among SACs, the network may alter both the shape of and the synchrony among the intrinsic bursts in SACs, thereby regulating the rhythm and the pattern of retinal waves. Several important features of this network seem consistent with a previous model of retinal waves[45]. The detailed mechanism for wave initiation and rhythmogenesis awaits further experimental and computational studies.

The mechanism underlying the intrinsic activity in SACs

The finding that I_{sAHP} or an I_{sAHP}-like current underlies the AHP following an intrinsic burst in SACs demonstrated that this current has a critical role in the refractory process of early network oscillation. Unlike most pacemaker neurons, which often rely on pacemaker currents such as I_H, T-type Ca^{2+} and persistent sodium (Na^{2+}) currents to generate the ramp (rebound) depolarization from the AHP (refs. 11,38–40), SACs seemed to rely largely on the decay of I_{sAHP} to produce the slow depolarization that brought the cell from AHP to the spike threshold (although it is possible that other channels also contributed to the ramp depolarization, especially at membrane potentials near the threshold for spikes). I_{sAHP} is modulated by a rich variety of neurotransmitters and protein kinases[28–30]. Our results indicated that I_{sAHP} in SACs provides an important site for network regulation and experimental manipulation of the spatiotemporal pattern of retinal waves. It will be important to understand how the membrane potential, Ca^{2+}, cAMP and perhaps other factors interact with each other in SACs to regulate retinal waves.

I_{sAHP} is also affected by intracellular dialysis during whole-cell patch clamp. In particular, Ca^{2+} chelators and anions (for example, the chloride ion (Cl^-), gluconate and methylsulfate) have paradoxical effects on this current[41–43]. Thus the measurement of burst kinetics (for example, AHP duration and interburst interval) could have been influenced by the experimental condition. To minimize some of these effects, we used pipette solutions that contained a low concentration (0.2 mM) of EGTA (see Methods). We found that prolonged (>15 min) whole-cell recording often led to a gradual hyperpolarization and disappearance of intrinsic bursts in SACs, perhaps as a result of intracellular dialysis; this may also explain, at least in part, why previous recordings did not detect the intrinsic bursts in SACs[21].

We found that about 60% of SACs recorded under whole-cell patch clamp showed spontaneous rhythmic bursts. The absence of detectable bursts in the remaining SACs might be caused, at least partly, by technical reasons, such as intracellular dialysis and the health of the cells, although we cannot rule out the possibility that only a subpopulation of SACs have intrinsic rhythmic activity. We also found that intrinsic Ca^{2+} bursts in SACs recorded in the antagonist cocktail under Ca^{2+} imaging seemed less regular than the intrinsic bursts recorded under whole-cell patch clamp. Thus, future studies should investigate what might have contributed to this difference. Our Ca^{2+} imaging experiments occasionally found that, in addition to SACs, some non-starburst amacrine cells also had intrinsic bursting activities, consistent with the finding of intrinsic bursts in some cultured neurons (predominantly non-starburst GABAergic cells) isolated from the developing rat retina (S.I. Firth & M.B. Feller, *Invest. Ophthalmol. Vis. Sci. Abstr.* 45.5331, 2004). However, because stage II waves in the rabbit depend critically on nicotinic transmission and are not affected by GABA receptor blockers[15], we believe the waves seen in E29–P4 rabbits originate from the intrinsic activity of SACs.

Our finding of the developmental loss of intrinsic bursts in SACs may explain why the intrinsic bursting activity has not been found in mature SACs (SACs in the mature mouse retina receive ~3 Hz glutamatergic synaptic input but do not show intrinsic oscillatory activity; ref. 44). The rapid disappearance of intrinsic activity in SACs coincided with three other developmental transitions in the retina: (i) a switch of spontaneous retinal waves from stage II to stage III (refs. 15,18); (ii) a rapid developmental reduction of reciprocal nicotinic synapses between SACs (ref. 14); and (iii) a switch from excitatory to inhibitory GABAergic interactions in the inner rabbit retina[14,15]. Thus, the generation of intrinsic bursts in individual SACs was coordinated with the amplification, synchronization, propagation and regulation of these activities, all of which require recurrent starburst network interactions. Likewise, the disappearance of intrinsic bursts in SACs after P6 was also coordinated with the dismantling of recurrent excitation in the SAC network, so that the same SACs may have a different role in visual processing.

METHODS

Electrophysiology. Patch-clamp recordings were made from displaced SACs and ganglion cells in flat-mount retinas of New Zealand white rabbits aged E29 to P29 as described[14,21]. All procedures involving the use of animals were according to National Institutes of Health guidelines. Whole-cell and on-cell patch-clamp recordings were made with EPC9-2 (Heka Elektronic) or Multiclamp 700A (Axon Instruments) amplifiers under a 40× (0.8 NA) or 60×

(0.9 NA) water immersion lens on an upright microscope (BX50WI, Olympus). The retina was continuously superfused (3–4 ml min^{-1}) with Ames medium at 34–37 °C. When Cd^{2+} was used, $NaHCO_3$ in Ames Medium was replaced by 20 mM HEPES. Sulforhodamine 101 was supplemented in the pipette solutions for identification of cell types. Cells recorded with on-cell patch clamp or Ca^{2+} imaging were identified by intracellular Lucifer yellow injection at the end of the recording. The pipette solution for whole-cell current clamp contained 115 mM potassium gluconate, 5 mM KCl, 2 mM $MgCl_2$, 5 mM NaOH, 0.2 mM EGTA, 2 mM adenosine 5′-triphosphate (disodium salt), 0.5 mM guanosine 5′-triphosphate (trisodium salt), 10 mM HEPES buffer and 2 mM ascorbate (pH 7.2). The pipette solution for voltage clamp contained 110 mM $CsMeSO_4$, 0.5 mM $CaCl_2$, 2 mM $MgCl_2$, 5 mM NaOH, 5 mM EGTA, 2 mM adenosine 5′-triphosphate (disodium salt), 0.5 mM guanosine 5′-triphosphate (trisodium salt), 10 mM HEPES buffer and 2 mM ascorbate (pH 7.2, with CsOH). On-cell, loose patch recordings were made with pipettes containing Ames medium. The pipette solution for Ca^{2+} and cAMP uncaging experiments was the same as that for the whole-cell current clamp, except that $MgCl_2$ and EGTA were omitted. Caged cAMP (100 μM) or DM-nitrophen (10 mM, loaded with Ca^{2+} to ~80%) was added directly to the pipette solution. Ultraviolet flashes were generated by a flash lamp (Model JML-C2, Rapp Optoelectronic) and delivered to the retina via a 40× water immersion lens (0.8 NA) as described[14]. Whole-cell patch-clamp data were low-pass filtered at 2 kHz (f_c), whereas on-cell recording data were band-pass filtered between 0.05 Hz and 2 kHz.

Calcium imaging. Isolated E29–P1 retinas were loaded with Fura-2AM (10 μM) as described[18]. Ganglion and displaced amacrine cells were imaged at 380 nm excitation and 500 nm emission wavelengths under a 40× objective lens (0.8 NA) with a CCD camera (Coolsnap HQ, Roper Scientific). Fractional changes in emission intensity, $\Delta F/F$, were measured from individual cell bodies and analyzed with MetaImaging software (Molecular Devices; ref. 18). Cross-correlation analysis was made with pClamp software (Axon Instruments). All data were expressed as mean ± s.d. unless noted otherwise.

Note: Supplementary information is available on the Nature Neuroscience website.

ACKNOWLEDGMENTS

We thank Q. Yang and T. Mon for help with some imaging experiments and A. Hayar for discussions on cross-correlation analysis. This study was supported by US National Institutes of Health grant R01EY10894 (to Z.J.Z.), unrestricted funds from Research to Prevent Blindness Inc. and from the Pat and Willard Walker Eye Research Center, and by the University of Arkansas for Medical Sciences Tobacco Fund.

COMPETING INTERESTS STATEMENT

The authors declare that they have no competing financial interests.

Published online at http://www.nature.com/natureneuroscience/
Reprints and permissions information is available online at http://npg.nature.com/reprintsandpermissions/

1. Wong, R.O. Retinal waves and visual system development. *Annu. Rev. Neurosci.* **22**, 29–47 (1999).
2. Torborg, C.L. & Feller, M.B. Spontaneous patterned retinal activity and the refinement of retinal projections. *Prog. Neurobiol.* **76**, 213–235 (2005).
3. Stellwagen, D. & Shatz, C.J. An instructive role for retinal waves in the development of retinogeniculate connectivity. *Neuron* **33**, 357–367 (2002).
4. Torborg, C.L., Hansen, K.A. & Feller, M.B. High frequency, synchronized bursting drives eye-specific segregation of retinogeniculate projections. *Nat. Neurosci.* **8**, 72–78 (2005).
5. McLaughlin, T., Torborg, C.L., Feller, M.B. & O'Leary, D.D. Retinotopic map refinement requires spontaneous retinal waves during a brief critical period of development. *Neuron* **40**, 1147–1160 (2003).
6. Grubb, M.S., Rossi, F.M., Changeux, J.P. & Thompson, I.D. Abnormal functional organization in the dorsal lateral geniculate nucleus of mice lacking the beta 2 subunit of the nicotinic acetylcholine receptor. *Neuron* **40**, 1161–1172 (2003).
7. Chandrasekaran, A.R., Plas, D.T., Gonzalez, E. & Crair, M.C. Evidence for an instructive role of retinal activity in retinotopic map refinement in the superior colliculus of the mouse. *J. Neurosci.* **25**, 6929–6938 (2005).
8. Mrsic-Flogel, T.D. *et al.* Altered map of visual space in the superior colliculus of mice lacking early retinal waves. *J. Neurosci.* **25**, 6921–6928 (2005).
9. Feller, M.B. Spontaneous correlated activity in developing neural circuits. *Neuron* **22**, 653–656 (1999).
10. O'Donovan, M.J. The origin of spontaneous activity in developing networks of the vertebrate nervous system. *Curr. Opin. Neurobiol.* **9**, 94–104 (1999).
11. Luthi, A. & McCormick, D.A. H-current: properties of a neuronal and network pacemaker. *Neuron* **21**, 9–12 (1998).
12. Ramirez, J.M., Tryba, A.K. & Pena, F. Pacemaker neurons and neuronal networks: an integrative view. *Curr. Opin. Neurobiol.* **14**, 665–674 (2004).
13. Buzsaki, G. & Draguhn, A. Neuronal oscillations in cortical networks. *Science* **304**, 1926–1929 (2004).
14. Zheng, J.J., Lee, S. & Zhou, Z.J. A developmental switch in the excitability and function of the starburst network in the mammalian retina. *Neuron* **44**, 851–864 (2004).
15. Syed, M.M., Lee, S., Zheng, J. & Zhou, Z.J. Stage-dependent dynamics and modulation of spontaneous waves in the developing rabbit retina. *J. Physiol. (Lond.)* **560**, 533–549 (2004).
16. Bansal, A. *et al.* Mice lacking specific nicotinic acetylcholine receptor subunits exhibit dramatically altered spontaneous activity patterns and reveal a limited role for retinal waves in forming ON and OFF circuits in the inner retina. *J. Neurosci.* **20**, 7672–7681 (2000).
17. Feller, M.B., Wellis, D.P., Stellwagen, D., Werblin, F.S. & Shatz, C.J. Requirement for cholinergic synaptic transmission in the propagation of spontaneous retinal waves. *Science* **272**, 1182–1187 (1996).
18. Zhou, Z.J. & Zhao, D. Coordinated transitions in neurotransmitter systems for the initiation and propagation of spontaneous retinal waves. *J. Neurosci.* **20**, 6570–6577 (2000).
19. Wong, W.T., Myhr, K.L., Miller, E.D. & Wong, R.O. Developmental changes in the neurotransmitter regulation of correlated spontaneous retinal activity. *J. Neurosci.* **20**, 351–360 (2000).
20. Zhou, Z.J. The function of the cholinergic system in the developing mammalian retina. *Prog. Brain Res.* **131**, 599–613 (2001).
21. Zhou, Z.J. Direct participation of starburst amacrine cells in spontaneous rhythmic activities in the developing mammalian retina. *J. Neurosci.* **18**, 4155–4165 (1998).
22. Ames, A. & Nesbett, F.B. In vitro retina as an experimental model of the central nervous system. *J. Neurochem.* **37**, 867–877 (1981).
23. Stellwagen, D., Shatz, C.J. & Feller, M.B. Dynamics of retinal waves are controlled by cyclic AMP. *Neuron* **24**, 673–685 (1999).
24. Faber, E.S. & Sah, P. Calcium-activated potassium channels: multiple contributions to neuronal function. *Neuroscientist* **9**, 181–194 (2003).
25. Lancaster, B. & Adams, P.R. Calcium-dependent current generating the afterhyperpolarization of hippocampal neurons. *J. Neurophysiol.* **55**, 1268–1282 (1986).
26. Lancaster, B. & Nicoll, R.A. Properties of two calcium-activated hyperpolarizations in rat hippocampal neurones. *J. Physiol. (Lond.)* **389**, 187–203 (1987).
27. Sah, P. & Clements, J.D. Photolytic manipulation of $[Ca^{2+}]i$ reveals slow kinetics of potassium channels underlying the afterhyperpolarization in hippocampal pyramidal neurons. *J. Neurosci.* **19**, 3657–3664 (1999).
28. Sah, P. Ca(2+)-activated K+ currents in neurones: types, physiological roles and modulation. *Trends Neurosci.* **19**, 150–154 (1996).
29. Sah, P. & Faber, E.S. Channels underlying neuronal calcium-activated potassium currents. *Prog. Neurobiol.* **66**, 345–353 (2002).
30. Vogalis, F., Storm, J.F. & Lancaster, B. SK channels and the varieties of slow after-hyperpolarizations in neurons. *Eur. J. Neurosci.* **18**, 3155–3166 (2003).
31. Shah, M.M., Miscony, Z., Javadzadeh-Tabatabaie, M., Ganellin, C.R. & Haylett, D.G. Clotrimazole analogues: effective blockers of the slow afterhyperpolarization in cultured rat hippocampal pyramidal neurones. *Br. J. Pharmacol.* **132**, 889–898 (2001).
32. Ozaita, A. *et al.* A unique role for Kv3 voltage-gated potassium channels in starburst amacrine cell signaling in mouse retina. *J. Neurosci.* **24**, 7335–7343 (2004).
33. Sipila, S.T., Huttu, K., Soltesz, I., Voipio, J. & Kaila, K. Depolarizing GABA acts on intrinsically bursting pyramidal neurons to drive giant depolarizing potentials in the immature hippocampus. *J. Neurosci.* **25**, 5280–5289 (2005).
34. Tauchi, M. & Masland, R.H. The shape and arrangement of the cholinergic neurons in the rabbit retina. *Proc. R. Soc. Lond. B* **223**, 101–119 (1984).
35. Vaney, D.I. 'Coronate' amacrine cells in the rabbit retina have the 'starburst' dendritic morphology. *Proc. R. Soc. Lond. B* **220**, 501–508 (1984).
36. Famiglietti, E.V. Starburst amacrine cells: morphological constancy and systematic variation in the anisotropic field of rabbit retinal neurons. *J. Neurosci.* **5**, 562–577 (1985).
37. Feller, M.B., Butts, D.A., Aaron, H.L., Rokhsar, D.S. & Shatz, J.C. Dynamic processes shape spatiotemporal properties of retinal waves. *Neuron* **19**, 293–306 (1997).
38. Jackson, A.C., Yao, G.L. & Bean, B.P. Mechanism of spontaneous firing in dorsomedial suprachiasmatic nucleus neurons. *J. Neurosci.* **24**, 7985–7998 (2004).
39. McCormick, D.A. & Huguenard, J.R. A model of the electrophysiological properties of thalamocortical relay neurons. *J. Neurophysiol.* **68**, 1384–1400 (1992).
40. Huguenard, J.R. & McCormick, D.A. Simulation of the currents involved in rhythmic oscillations in thalamic relay neurons. *J. Neurophysiol.* **68**, 1373–1383 (1992).
41. Schwindt, P.C., Spain, W.J. & Crill, W.E. Effects of intracellular calcium chelation on voltage-dependent and calcium-dependent currents in cat neocortical neurons. *Neuroscience* **47**, 571–578 (1992).
42. Zhang, L. *et al.* Potentiation of a slow Ca(2+)-dependent K+ current by intracellular Ca2+ chelators in hippocampal CA1 neurons of rat brain slices. *J. Neurophysiol.* **74**, 2225–2241 (1995).
43. Velumian, A.A. & Carlen, P.L. Differential control of three after-hyperpolarizations in rat hippocampal neurones by intracellular calcium buffering. *J. Physiol. (Lond.)* **517**, 201–216 (1999).
44. Petit-Jacques, J., Volgyi, B., Rudy, B. & Bloomfield, S.A. Spontaneous oscillatory activity of starburst amacrine cells in the mouse retina. *J. Neurophysiol.* **94**, 1770–1780 (2005).